Journal of Controlled Release 197 (2015) 148–157

Contents lists available at ScienceDirect

Journal of Controlled Release

journal homepage: www.elsevier.com/locate/jconrel

Release and bioactivity of bone morphogenetic protein-2 are affected by scaffold binding techniques *in vitro* and *in vivo*

Salwa Suliman [a,*,1], Zhe Xing [a,1], Xujun Wu [b], Ying Xue [a], Torbjorn O. Pedersen [a], Yang Sun [c], Anne P. Døskeland [d], Joachim Nickel [e,f], Thilo Waag [i], Henning Lygre [g], Anna Finne-Wistrand [c], Doris Steinmüller-Nethl [h], Anke Krueger [i], Kamal Mustafa [a,*]

[a] *Department of Clinical Dentistry, Center for Clinical Dental Research, University of Bergen, Norway*
[b] *Department of Cranio-Maxillofacial and Oral Surgery, Medical University of Innsbruck, Innsbruck, Austria*
[c] *Department of Fibre and Polymer Technology, Royal Institute of Technology, KTH, Stockholm, Sweden*
[d] *Department of Biomedicine, University of Bergen, Norway*
[e] *Chair Tissue Engineering and Regenerative Medicine, University Hospital of Würzburg, Germany*
[f] *Fraunhofer Project Group Regenerative Technologies in Oncology, Würzburg, Germany*
[g] *Department of Clinical Science, University of Bergen, Bergen, Norway*
[h] *DiaCoating GmbH, Innsbruck, Austria*
[i] *Institute of Organic Chemistry, University of Würzburg, Würzburg, Germany*

ARTICLE INFO

Article history:
Received 27 June 2014
Accepted 3 November 2014
Available online 10 November 2014

Chemical compounds studied in this article:
L-lactide (PubChem CID: 107983)
Caprolactone (PubChem CID 10401)
Benzoquinone (PubChem CID: 4650)

Keywords:
Drug delivery
Functionalization
Growth factor
Nanodiamond
Copolymer scaffold
Tissue engineering

ABSTRACT

A low dose of 1 μg rhBMP-2 was immobilised by four different functionalising techniques on recently developed poly(L-lactide)-co-(ε-caprolactone) [(poly(LLA-co-CL)] scaffolds. It was either (i) physisorbed on unmodified scaffolds [PHY], (ii) physisorbed onto scaffolds modified with nanodiamond particles [nDP-PHY], (iii) covalently linked onto nDPs that were used to modify the scaffolds [nDP-COV] or (iv) encapsulated in microspheres distributed on the scaffolds [MICS]. Release kinetics of BMP-2 from the different scaffolds was quantified using targeted mass spectrometry for up to 70 days. PHY scaffolds had an initial burst of release while MICS showed a gradual and sustained increase in release. In contrast, NDP-PHY and nDP-COV scaffolds showed no significant release, although nDP-PHY scaffolds maintained bioactivity of BMP-2. Human mesenchymal stem cells cultured *in vitro* showed upregulated BMP-2 and osteocalcin gene expression at both week 1 and week 3 in the MICS and nDP-PHY scaffold groups. These groups also demonstrated the highest BMP-2 extracellular protein levels as assessed by ELISA, and mineralization confirmed by Alizarin red. Cells grown on the PHY scaffolds *in vitro* expressed collagen type 1 alpha 2 early but the scaffold could not sustain rhBMP-2 release to express mineralization. After 4 weeks post-implantation using a rat mandible critical-sized defect model, micro-CT and Masson trichrome results showed accelerated bone regeneration in the PHY, nDP-PHY and MICS groups. The results demonstrate that PHY scaffolds may not be desirable for clinical use, since similar osteogenic potential was not seen under both *in vitro* and *in vivo* conditions, in contrast to nDP-PHY and MICS groups, where continuous low doses of BMP-2 induced satisfactory bone regeneration in both conditions. The nDP-PHY scaffolds used here in critical-sized bone defects for the first time appear to have promise compared to growth factors adsorbed onto a polymer alone and the short distance effect prevents adverse systemic side effects.

1. Introduction

Reconstruction of critical-sized bone defects continues to be a challenge. The limitations of current treatment methods [1] highlight the importance of introducing a potent bone substitute or a scaffold that can induce bone healing by unlocking the body's own powers of self-repair; not only should the substrate be osteo-inductive, it must also act as a delivery system for the regenerative cues necessary [2]. The osteo-inductive capacity of the FDA approved recombinant human bone morphogenetic protein (rhBMP-2) in bone and cartilage formation has been confirmed in preclinical models [3] and evaluated in clinical trials [4]. It has usually been delivered in bolus injections with supra-physiological doses to attain a therapeutic effect, leading to severe side effects ranging from heterotopic bone to oedema or high morbidity in cases of spinal fusion [5]. The

* Corresponding authors at: Department of Clinical Dentistry, Center for Clinical Dental Research, Faculty of Medicine and Dentistry, University of Bergen, 5009 Bergen, Norway. Tel.: +47 55586356; fax: +47 55586568.
E-mail addresses: salwa.suliman@iko.uib.no (S. Suliman), kamal.mustafa@iko.uib.no (K. Mustafa).
[1] Contributed equally.

http://dx.doi.org/10.1016/j.jconrel.2014.11.003

high doses of rhBMP-2 chosen were used to compensate for short half-life *in vivo* (1–4 h) [6,7].

Many studies have pursued the design of different carriers delivering BMP-2 including implant coatings or organic and inorganic matrices [8–10]. Control over its bioactivity and spatial–temporal presence is essential for a beneficial effect but has been difficult to achieve [1]. To improve the unsatisfactory outcomes resulting from bolus delivery of BMP-2, attempts have been made to develop biomaterial carriers that maintain a sufficient concentration at the application site to stimulate the normal physiological mechanism required for bone regeneration [11]. Adsorption to collagen sponges and soaking of collagen sponges and hydrogels in BMP-2 are the most commonly used potential carrier approaches due to their high binding capacities and successful induction of trabecular bone volume in critical defects of the canine has been reported [12]. Recent reports using FDA approved polymers, such as poly(lactide-co-glycolide) (PLGA) and polycaprolactone (PCL) have looked at functionalising with BMP-2 [13] due to the affinity of rhBMP-2 for molecules such as heparin or RGD peptides [14]. Covalent immobilisation of BMP-2 to biomaterials modified with heparin, plasma treatment, UV light or disulphide bonds [15,16] has also been examined in attempts to improve the stability and increase retention in regeneration sites by reducing the release of BMP-2 and sustaining its activity.

The introduction of micro- and nano-structured materials has been shown to increase the surface area of scaffolds, allowing for numerous non-covalent interactions between the scaffold surface and protein [17]. Protein encapsulation within microspheres is a potent tool to protect its biological activity and enable sustained release over longer periods [18]. PLGA has generated great interest as a copolymer for microsphere fabrication due to its biocompatibility as well as the ability to tailor its *in vivo* lifetime [11]. This can be achieved by varying the polymer molecular weight, composition, microsphere size and distribution. Several studies have shown that the rate of release depends on the microsphere size, therefore by mixing particles with different sizes one can obtain a degree of control over release [19]. This control of the release profile of growth factors results in optimised concentrations for growth, making it suitable for experimental designs lasting for a long term.

Surface coatings with diamonds at the nano-level gained significance in the medical field after it was shown to demonstrate chemical stability, and to enhance mechanical properties and biocompatibility [20]. In recent years, research has focused on nano-topographic surface modifications aiming to allow for numerous non-covalent interactions between the surface and protein, resulting in adsorbed protein layers which in turn increase cellular adhesion and durability of biomedical implants [21,22], improving various biological applications including delivery of growth factors [23,24]. Previous work showed enhanced cellular response through coating with nanocrystalline diamond (NCD) films [25]. NCD modified titanium dental implant surfaces with terminal oxygen groups that interacted strongly with rhBMP-2 allowing the physisorption of BMP-2. This was demonstrated by greatly enhanced osseointegration [26]. Nanodiamond particles (nDPs) provided enhanced surface properties enhancing bone formation [27,28], encouraging further studies of binding growth factors onto nDP to evaluate their bioactivity.

Long-term delivery of BMP-2 in mini pig models proved enhancement of *in vivo* osteogenic efficacy of the protein compared to short-term delivery [29], while burst release has shown significance in an ectopic bone-forming model using transplanted hydrogels [30] rather than in long-term osteogenic activity. It is, however, difficult to compare these approaches due to the variety in animal models, doses and delivery vehicles used, although collectively, they have resulted in understanding how to design an optimum delivery system. Therefore, since the release of BMP-2 and its effect on the tissues depend on the carrier, method of immobilisation and subsequent mode of delivery, the release kinetics and osteoinductive capacity of different loading approaches need further evaluation.

Degradable poly(L-lactide-co-ε-caprolactone) [Poly(LLA-co-CL)], an aliphatic polyester, copolymer of L-lactide and ε-caprolactone has been extensively studied as a scaffold for bone regeneration [31,32] proving its biocompatibility and osteoconductivity. Mechanical and surface properties can be modified [33] to enhance the regenerative potential, and functionalisation of these scaffolds with nDP to improve cellular response and subsequent bone formation has been reported [28].

In an effort to further improve these scaffolds, the aim of the current study was to study the effect of rhBMP-2 in low amount (1 μg) immobilised on poly (LLA-co-CL) scaffolds utilising four different methods. The release kinetics of rhBMP-2 from the different methods was first quantified *in vitro* and bioactivity evaluated on human mesenchymal stem cells (hMSCs) and then the osteogenic effect of these different methods was further compared *in vivo*.

2. Materials and methods

2.1. Poly(LLA-co-CL) scaffold fabrication (CL scaffold)

Scaffolds were fabricated as previously described [31]. Scaffolds were punched out in two different dimensions for *in vitro* and *in vivo* experiments (*in vitro*: 12 mm diameter and 1.3 mm thickness) and (*in vivo*: 6 mm diameter and 2.5 mm thickness).

2.2. Scaffold functionalisation and BMP-2 immobilisation techniques

2.2.1. BMP-2 production

BMP-2 cDNA was prepared corresponding to residues 283–396 of the mature protein plus an N-terminal MA extension. The BMP-2 protein was expressed in *Escherichia coli* (*E. coli*), isolated from inclusion bodies, renatured and purified as previously described [34]. One microgram of BMP-2 was used per scaffold for each type of functionalisation for *in vitro* with hMSC and *in vivo* experiments.

2.2.2. Physisorbed BMP-2 (PHY scaffold)

BMP-2 was physisorbed onto unmodified poly(LLA-co-CL) scaffolds as follows: scaffolds were placed on a sterilised hydrophobic surface (M Barrier Film, Parafilm®) and 1 μg of BMP-2/50 μl phosphate buffered saline (PBS) was dropped in two increments of 25 μl each onto the surface of the scaffold. The first aliquot was allowed to adsorb under humid shaking conditions for 30 min, after which the second aliquot was added and left for 30 min before the scaffold was used for *in vitro* or *in vivo* experiments.

2.2.3. Colloidal nDP production

Acid purified detonation diamond (Gansu Lingyun Corp. Lanzhou, China) was subjected to attrition milling using a method previously described [35] achieving a narrow size distribution at ~5 nm particle diameter (measured by dynamic light scattering in water) and low agglomeration of the diamond particles.

2.2.4. Scaffolds modified with nDP and physisorbed with BMP-2 (nDP-PHY scaffold)

Scaffolds were modified with the nDP solution (2% (w/v), i.e. 20 mg/ml) by a vacuum technique: 0.5 ml nDP solution and one scaffold were put in a glass beaker and perfused in vacuum. The vacuum chamber was evacuated down to the pressure where the nDP-water-solution changes into the vapour phase and the nDP burst into the scaffold surface. This cycle was repeated 10 times. After the modification, the nDP modified scaffolds were rinsed with distilled water and dried in vacuum for 8 h. Brunauer–Emmett–Teller (BET) method using Argon at 87 K according to DIN ISO 9277 was performed to quantify the amount of nDP on the porous scaffold and the concentration of nDP was determined to be 14 mg in 1 g scaffold material. To physisorb the BMP-2, the modified scaffolds were treated with aforementioned protocol for PHY.

2.2.5. nDP functionalisation with BMP-2 (nDP-COV scaffold)

To functionalise nDP with benzoquinone, 189 mg of mechanically de-agglomerated nDP was suspended in 20 ml of PBS (pH 8) and 150 mg of benzoquinone (1.38 mmol) was added (all from VWR International, Radnor, PA, US). After stirring for 24 h at room temperature (RT) the reaction mixture was centrifuged and the nDP was washed with PBS (pH 7.4) and deionized water. Then nDP scaffolds were functionalised with BMP-2 by suspending 20 mg of benzoquinone-functionalised nDP in 15 ml of PBS buffer (pH 6). After adding 10 μg BMP-2 the reaction mixture was stirred for 24 h at RT. The nDP was centrifuged and then the supernatant was checked for residual BMP-2 and then discarded. The precipitate was washed with PBS (pH 7.4) and deionized water. The scaffolds were then modified with the functionalised nDP according to the procedure described in Section 2.2.4.

2.2.6. Microsphere preparation and scaffold modification (MICS scaffold)

BMP-2-loaded PLGA5050 (Purac Biochem, Gorinchem, Netherlands) microspheres were fabricated using a previously described water-in-oil-in-water double emulsion solvent extraction technique [11,36]. Briefly, 1 ml of a 50 μg/ml BMP-2 solution was emulsified in a solution of 15% (w/v) PLGA5050 in 5 ml of dichloromethane using a probe ultrasonicator (Branson sonifier cell disruptor 200, USA). The mixture was then immediately re-emulsified for 60 s in 10 ml of a 1% w/v aqueous poly(vinyl alcohol) (PVA, 87–89 mol% hydrolysed, Mw = 13,000–23,000) solution to create the double emulsion. The product was then added to 100 ml of a 0.5% w/v aqueous PVA solution and 100 ml of a 2% w/v aqueous isopropanol solution and stirred for 2 h. The microspheres were centrifuged, washed 5 times and vacuum dried into a free flowing powder (Braun Biotech International SpeedVac Concentrator SVC 10H Savant, USA). BMP-2 loaded microspheres were incorporated into the porous poly(LLA-co-CL) scaffold using a seeding technique described previously [37] with slight modifications. Depending on the amount of BMP-2 for loading, dry microspheres were dispersed in 100 μl ethanol using an ultrasonic bath (VWR International). Fifty microlitres of the microsphere suspension was placed onto both sides of the scaffold and dried overnight under vacuum.

The loading efficiency of the microspheres was determined using a solvent-extraction technique [38]. Approximately 20 mg of microparticles was dissolved in 1 ml of dichloromethane for 6 h at 37 °C. The entrapped rhBMP-2 was extracted from the organic phase to the aqueous phase by incubation with 5 ml of PBS for an additional 24 h. The concentration of rhBMP-2 was analysed by a commercially available human BMP-2 enzyme-linked immunosorbent assay (ELISA) (RnD Systems, Minneapolis, Minnesota, USA). The average loading efficiency was 0.04%. This optimization method was performed three times. Accordingly the amount of microspheres needed to contain exactly 1 μg of BMP-2 from loading efficiency is calculated, i.e 2.5 mg microparticles contains 1 μg, each optimisation added 2.5 mg to the scaffold.

2.3. In vitro BMP-2 release kinetics

Scaffolds were immersed in 1 ml of PBS in glass test tubes (Duran®, Wertheim, Germany) and incubated in a shaking water bath (Julabo®, SW22, Germany) at 37 °C. Half of the supernatant was collected and replaced with fresh PBS at predetermined time points up to 70 days.

2.4. Sample preparation for selected reaction monitoring (SRM) analysis

rhBMP-2 (residues 283–396) expressed in *E. coli* was purchased (RELIATech GmbH, Wolfenbüttel, Germany). Four peptides derived from the 26 kDa protein by trypsinisation were tested for SRM analysis. Only one peptide NYQDMVVEGCGCR representative of BMP-2 revealed good transitions and was therefore selected for relative quantification of the protein. A stable isotope-labelled internal standard (SIS) corresponding to that signature peptide was purchased in AQUA QuantPro quality (Thermo Fisher Scientific, Waltham, MA, USA). The C-terminal arginine for the SIS was labelled with ^{13}C and ^{15}N resulting in a mass difference of 10 Da to the corresponding non-labelled peptide. In addition, cysteine was carbamidomethylated and methionine was oxidized. The chemically synthesised modified peptides were reported to be stable by the manufacturer. The peptide was optimised by direct infusion on a Q-Trap 5500 (AB SCIEX, MA, USA). Twenty five femtomole of SIS peptide NYQDMVVEGCGCR was spiked into samples containing unknown amounts of BMP-2 in low-binding tubes (LoBind, Eppendorf). The mixture was lyophilised (Centrivap® Centrifugal, USA) prior to in-solution protein digestion according to the protocol described previously (http://www.uib.no/file-archive/in-solution-proteindigestion.pdf). Prior to liquid chromatography SRM-mass spectrometry (LC SRM-MS) analysis, the mixtures of reduced and alkylated tryptic peptides were desalted using reverse phase Oasis® HLBμElution Plate 30 μm (Waters, Milford, MA, USA) as described previously [39]. The eluted peptides were dried in a speed vacuum drier and finally suspended in 8 μl of 1% FA and 2% ACN. In order to oxidize all methionine residues, H_2O_2 was added in a final concentration of 0.5%, and the samples were incubated for 30 min at 30 °C. The experiment was performed in triplicate. For each measurement, slightly different SRM methods were used and improved progressively to measure the release with addition of heavy peptide. The data shown in Fig. 1 were obtained with the most optimised SRM method, considered the most robust and representative of the conclusion derived from all measurements performed.

2.5. SRM analysis

LC SRM-MS analysis was performed on a Q-Trap 5500 coupled to a Dionex Ultimate system (Thermo Scientific, MA, USA) as previously described [39]. The protein digest was dissolved in 2% ACN, 0.1% FA and loaded into the instrument. For quantification of the signature peptide from BMP-2, all y transitions with significant intensity were used and a mean of the ratio values calculated to obtain ratio Light/Heavy (L/H). The Q1 values for the light peptide were 802.319, that for the SIS heavy labelled peptide 807.32. The collision energy used for SRM analysis was 45.5 eV. The raw data files generated were processed using Skyline (MacCoss Lab Software version 2.5).

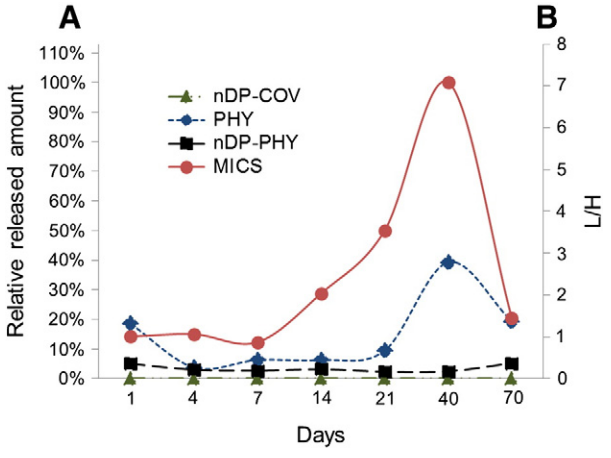

Fig. 1. Release kinetics of BMP-2 measured by SRM. (Axis-A) Relative amount released where 100% value corresponds to the highest value observed for the total amount of BMP-2 measured at a specific time point. (Axis-B) Release over time of rhBMP-2 from the different scaffolds expressed by the ratio (L/H) between endogenous light (L) and heavy synthetic (H) peptide spiked-in our sample measured by SRM. The figure is a representative of the data from the most optimised SRM method obtained from triplicate measurements.

2.6. Cell maintenance and seeding

Primary hMSCs (StemCell™ Technologies, Vancouver, BC, Canada) were expanded in MSCGM™ complete medium (Lonza, Basel, Switzerland) following the manufacturer's instructions. Flow cytometry used to assess the cells' purity showed that >90% of cells expressed CD29, CD44, CD105, and CD166 and that they lacked expression of CD14, CD34, and CD45. Morphology of the hMSCs was assessed by a light microscope (Nikon TS100, Tokyo, Japan). Cells used in the experiments were from passages 3 to 6. The cells were seeded onto the scaffolds at a density of 2×10^5 per scaffold and allowed to distribute better by a plate shaker (MixMate® Eppendorf, Hamburg, Germany) for 5 min before incubation at 37 °C and 5% CO_2 [40]. Once the cells reached 80–90% confluence the medium was replaced with osteogenic medium (MSCGM™ complete medium plus 50 μg/ml ascorbic acid, 10^{-8} M dexamethasone, and 3.5 mM β-glycerophosphate) and changed every fourth day. All cultures were performed in triplicate and the experiments were repeated three times.

Human osteoblast-like cells (HOB) were used as a positive control for the *in vitro* mineralization staining (Alizarin red S) (Section 2.10). They were isolated from routine surgical samples from patients being treated at the Section for Oral and Maxillofacial Surgery, Department of Clinical Dentistry, University of Bergen and Haukeland University Hospital. The procedure was approved by the Ethics Committee at the University of Bergen. The protocol for isolation and expansion has been previously described [41].

2.7. Scanning electron microscope (SEM) analysis

Attachment and spreading of hMSC on scaffolds at 1 and 3 days after seeding were analysed by SEM (Jeol JSM 7400F, Tokyo, Japan), voltage of 10 kV as previously described [40].

2.8. Genes expressed by cultured hMSC in vitro

Total RNA was isolated from *in vitro* cultures at week 1 and week 3 using a Tissue RNA isolation kit (Maxwell®, Promega, Madison, WI, USA), and reverse transcribed according to the manufacturer's instructions using the High capacity cDNA Reverse Transcription Kit (Applied Biosystems®, Carlsbad, CA, USA). Real-time reverse transcription-polymerase chain reaction (RT-PCR) was performed as previously described [40]. Taqman® gene expression assays (Applied Biosystems®) were used to detect mRNA levels of glyceraldehyde-3-phosphate dehydrogenase (GAPDH), Antigen KI-67 (Ki-67), Runt-related transcription factor 2 (Runx2), BMP-2 receptor 1A (BMPRIA), BMP-2 receptor 2 (BMPRII), Alkaline phosphatase (ALP), Collagen type 1 alpha 2 (Col1α2), Bone morphogenetic protein-2 (BMP-2) and Osteocalcin (OC). The data were analysed with a comparative C_T method and GAPDH served as endogenous control. Unmodified scaffold (CL) at week 1 was the reference.

2.9. Enzyme-linked immunosorbent assay

The culture medium was collected at week 1 and week 3. Human BMP-2 ELISA Development Kit (900-M255, Peprotech, Rocky Hill, NJ, US) was used to measure extracellular and intracellular BMP-2 following the manufacturers' instructions. To measure the intracellular production of BMP-2, the scaffolds with cells from both time points were washed with PBS before incubation at 4 °C on a shaker for 20 min with 175 μl RIPA buffer (Thermo Scientific), 1× Halt™ Protease Inhibitor Cocktail and 1× Halt™ Phosphatase Inhibitor Cocktail (Thermo Scientific). This was followed by sonication for 5 min and then centrifugation for 20 min at 16,000 *g* at 4 °C. The extracted protein was collected and measured using a bicinchoninic acid assay (BCA) (Pierce BCA Protein Assay Kit, Thermo Scientific) following the manufacturer's instructions.

2.10. In vitro mineralization

The cell/scaffold constructs were harvested at week 1 of culture, washed thrice in PBS and fixed for 10 min in 4% paraformaldehyde (PFA) (Merck & Co, White House Station, NJ, USA). Alizarin red S staining was performed to determine matrix mineralization. Two percent of alizarin red S powder (Sigma Aldrich) was dissolved in distilled water and pH was adjusted to 4.2 with 0.5% ammonium hydroxide. Constructs were stained for 20 min and imaged with a Nikon TS100 microscope. HOB cells cultured on CL scaffolds for 1 week were used as a positive control.

2.11. Animal model of mandibular defects

Male Sprague–Dawley rats (300–350 g) were anaesthetised with isoflurane (IsobaVet®; Schering-Plough, Kenilworth, NJ, USA) combined with O_2 using a custom-made platform and mask. A 1 cm incision was made along the lower border of the mandible and after retracting the muscles a round-shaped bone defect (5 mm diameter) was created in the mandibular angle region. A trephine bur (Komet Medical, Lemgo, Germany) was used. The defect was filled with a scaffold ($n = 8$ for each experimental group). The muscles were repositioned and the skin closed with resorbable sutures (Vicryl Rapide 4-0; Ethicon, Somerville, NJ, USA). Animals were euthanised with an overdose of CO_2 after 2 and 4 weeks. Mandibles were dissected and the samples were stored in RNAlater (Invitrogen, Carlsbad, CA, USA) for RT-PCR, micro computed tomography (micro-CT) and histological analyses.

2.12. Gene expressions in vivo

Total RNA was isolated from *in vivo* scaffolds at 2 weeks. Taqman® gene expression assays (Applied Biosystems™, USA) were used to detect mRNA levels of GAPDH, ALP, OC, Runx2, Col1α2, BMP-2, Bone morphogenetic protein-4 (BMP-4), Tartrate-resistant acid phosphatase (TRAP) and Cathepsin K (CTSK). The data were analysed with a comparative C_T method and GAPDH served as endogenous control. CL served as reference.

2.13. Micro-CT analysis

The amount of bone formation within the defects was examined using micro-CT (micro-CT 40, Scanco Medical AG, Bruettisellen, Switzerland) with 19 μm isotropic voxel size and 70 kV, 43 μA tube current, 380 ms exposure time, and 1000 projections [42]. Three-dimensional isosurface rendering and images were constructed with the software provided by Scanco Medical and measurements included the ratio of new bone volume relative to the tissue volume (BV/TV).

2.14. Histological evaluation

Specimens for histological examination were processed as previously described [43]. Sections were then stained with Masson's trichome to confirm the osteoid-like tissue and images were made with an inverted microscope (Nikon Ti, Tokyo, Japan) using the software NIS-Elements AR 4.10.

2.15. Statistical analysis

The average values were analysed using SPSS Statistics 21.0 (IBM, Armonk, NY, US). The data were expressed as mean +/− standard deviation (SD). Data were tested for variance homogeneity and normal distribution and One-way ANOVA were followed by a multiple-

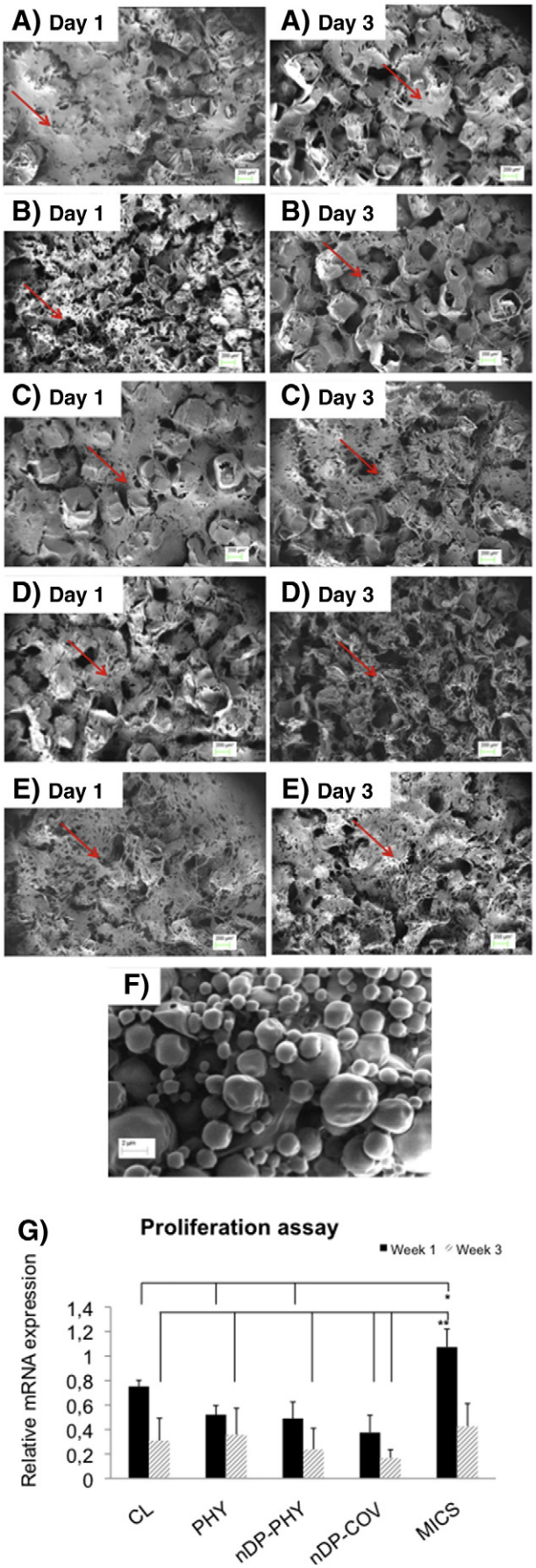

comparison Tukey test. Analysis of the *in vivo* experiment data was performed with the Kruskal–Wallis test. Differences between the means were considered statistically significant when $p < 0.05$.

3. Results

3.1. In vitro kinetics of BMP-2 release

The release of BMP-2 was monitored through identification of signature peptide NYQDMoxVVEGCcamGCcamR as analysed by SRM. The amount of a signature peptide (L, endogenous peptide) for BMP-2 is related to a known amount of internal standard (H, heavy synthetic peptide) spiked-in our sample, and the ratio (L/H) is used as an index for the amount of BMP-2 released (Fig. 1). The figure is a representative of the data from the most optimised SRM method obtained from triplicate measurements.

In the first 24 h, the PHY scaffolds had an initial burst of release. There was a steady release from the MICS scaffolds starting from 24 h while the nDP-COV scaffold group showed no release. MICS scaffolds showed a gradual increase in release from day 7 on, with the greatest release being found between days 21 and 40. In comparison to the MICS scaffolds, the PHY scaffolds showed a smaller increase in release between days 21 and 40, while the nDP-PHY scaffolds showed a maintained level.

3.2. hMSC attachment and proliferation

SEM images at day 1 and day 3 of culture show the spreading and attachment of hMSC on the different scaffolds. Significantly more cells on the MICS modified group were proliferating on day 7 compared to the other scaffold groups (Fig. 2 G).

3.3. BMP-2 signalling and hMSC differentiation

Similar results were seen between the groups (Fig. 3) for expression of the two main receptors of BMP-2 signalling (BMPRIA and BMPRII). Results showed the highest expression of receptor significantly from the MICS at 3 weeks ($p = 0.033$, $p = 0.029$). At week 1 the nDP-PHY group showed higher but not statistically significant expression compared with the PHY group, while at week 3 the PHY group showed a higher trend, coinciding with the release profile during that period, which was again not statistically significant. A tendency was seen for an increase in the master transcription factor Runx2 in all groups at week 3 compared to week 1 (Fig. 3). Col1α2 was upregulated in all groups at week 3 compared to week 1 except in the nDP-COV group, where it was downregulated. In all the other groups, ALP was upregulated at week 3 with nDP-PHY showing the highest tendency (Fig. 3). MICS and nDP-PHY showed the highest BMP-2 expression at both early and late time points (Fig. 3), although this was only significant in the MICS group at week 3. OC was significantly upregulated at week 3 in the MICS group followed by the nDP-PHY group, compared with the other groups.

3.4. In vitro endogenous BMP-2 protein expression

The medium was collected at week 1 and week 3 to determine the extracellular release of endogenous BMP-2 from hMSC. The BMP-2 ELISA kit used is sensitive to natural and mammalian-expressed BMP-

Fig. 2 Attachment and proliferation of hMSC cultured on the different scaffolds. SEM images at days 1 and 3 showing attachment of hMSCs (red arrows) (A) CL, (B) PHY, (C) nDP-PHY, (D) nDP-COV and (E) MICS. Scale bar = 200 μm. (F) Higher magnification of MICS scaffold without cells showing the increased surface area resulting from the microspheres. Scale bar = 2 μm. (G) The proliferative activity of the hMSC seeded onto the different scaffolds evaluated in terms of mRNA expression of the proliferative marker (Ki67) (*$p < 0.05$, **$p < 0.001$).

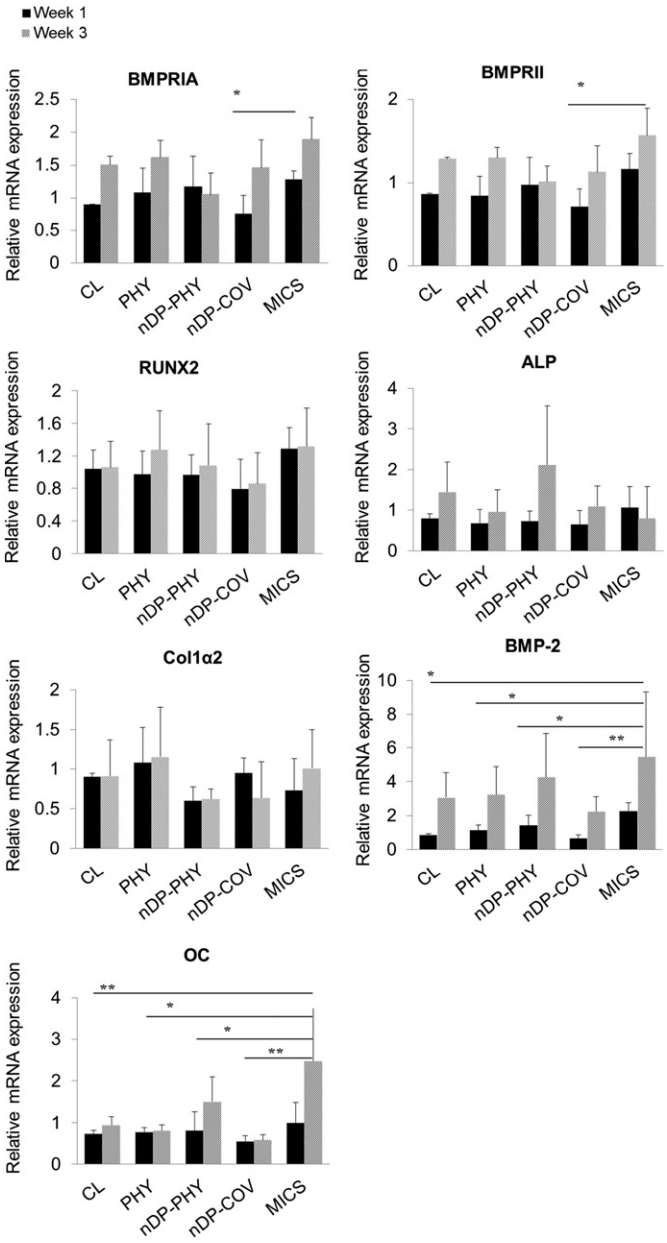

Fig. 3. Relative MRNA expression from hMSC cultured *in vitro* after week 1 and week 3. Relative mRNA levels of BMP-2 signalling receptors, transcription factor and osteogenic markers (*$p < 0.05$, **$p < 0.001$).

2 and does not recognize *E. coli*-expressed rhBMP-2. The levels detected here were therefore protein originating solely from hMSC. Extracellular endogenous BMP-2 showed the lowest expressions in the CL and nDP-COV groups, with minor differences between time points. The highest expression was seen from the MICS group at early and late time points and nDP-PHY at week 1 (Fig. 4A). Intracellular BMP-2 showed the highest levels in the MICS group at both time points and lowest in the nDP-PHY group (Fig. 4B). None were significant.

3.5. Alizarin red staining for in vitro mineralization

Staining revealed surface mineralization. Most groups showed variable reddish extracellular matrices while vast extracellular darker spots could be observed in the MICS and nDP-PHY group scaffolds as evidence of calcium deposits in the matrix (Fig. 5).

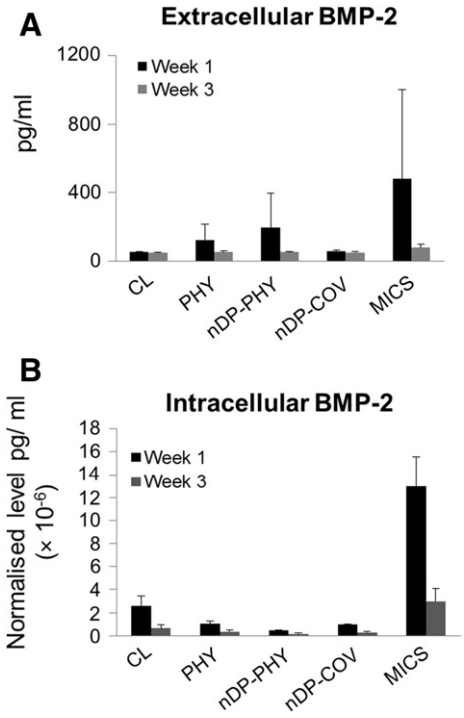

Fig. 4. *In vitro* endogenous BMP-2 protein expression by ELISA at week 1 and week 3. (A) for extracellular concentration of BMP-2 secreted in medium and (B) intracellular BMP-2.

3.6. Gene expressions from in vivo experiments

In vivo RT-PCR results showed coherence in several genes with the expressions *in vitro*. The transcription marker Runx2 showed the highest expression on the MICS scaffolds, although not significant. Significant upregulation of the early osteogenic marker ALP was expressed on MICS while COL1 was higher from the PHY scaffolds. OC was upregulated most on MICS scaffolds, followed by expression on nDP-PHY scaffolds, consistent with the *in vitro* results indicating deposition of bone matrix and mineralization. MICS scaffolds also demonstrated significant upregulation of the osteoclast markers TRAP and CTSK at 2 weeks.

3.7. De novo bone formation

Morphometric results with micro-CT show that most of the treated groups had increased bone volume inside the defined defect area compared to the empty group. Bone volume recover was greatest in the PHY and MICS groups at 4 weeks, and that both were significant in comparison to the nDP-COV scaffold group (Fig. 7A). They were followed by nDP-PHY.

Masson's trichrome staining was carried out to identify the osteoid-like tissue and collagen enriched areas in the defects. In the empty group (Fig. 7 B) it was predominantly soft tissues growing around and into the defect. The scaffold architecture was highly preserved in the CL and nDP-COV groups compared with other 3 functionalised scaffold groups. Most of the pores of the CL scaffolds were filled with loose fibrous connective tissue without much evidence of osteoid tissue formation. Histological results were in line with the micro-CT analysis showing mostly osteoid formation among the pores of the scaffolds in PHY, nDP-PHY and MICS at an early time point of 4 weeks (Fig. 7D, E and G).

4. Discussion

We evaluated the *in vitro* and *in vivo* efficacy of four different modes of rh-BMP-2 delivery utilising a low dose of 1 μg.

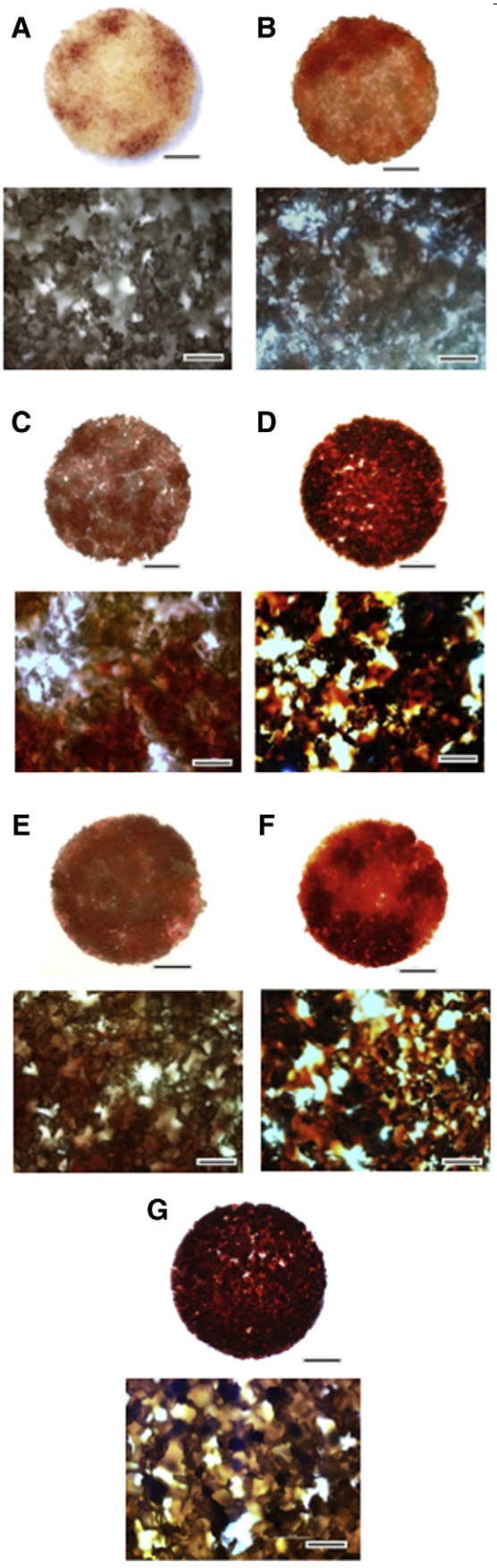

In vitro rhBMP-2 release from scaffolds was evaluated with targeted quantification using SRM and an absolute quantification method (AQUA). The SIS peptide was chemically identical to the native peptide with respect to retention time, ionization efficiency, and fragmentation characteristics. Its mass unit was higher and could therefore be distinguished from the native counterpart during MS analysis permitting the detection of very low concentrations [44]. In the PHY scaffold most of the BMP-2 was located superficially with weak bonds causing the initial burst release. A second increase in release from PHY was seen at a time point when the scaffold is beginning to degrade. This hypothesis is supported by the degradation profile from the same scaffold analysed by *in vitro* hydrolysis where forty days showed to be a sufficient time for significant reduction of its molecular weight contributing to increased degradation [45].

In contrast, the release of BMP-2 from MICS scaffolds was different. Several factors explain this difference, such as the microsphere size and its rate of degradation, which controlled the BMP-2 diffusion in a steadily increased fashion retaining the BMP-2 for an extended time. OC was highly expressed in cells grown on MICS at week 1 ($p < 0.05$) and week 3 *in vitro* and at 2 weeks *in vivo*, implying increased mineralization in comparison to that seen on PHY scaffolds. This demonstrates how long-term sustained delivery of BMP-2 enhances its osteogenic efficacy at the same dose compared to short-term delivery [46]. Differences in the initial burst release of BMP-2 from PHY and nDP-PHY scaffolds could be attributed to the lower amount of protein being only weakly bound to the scaffold in the case of nDP-PHY. No burst release was encountered as in PHY because the interaction of proteins with nDPs is known to be rather strong [47]. Also previous reports where spectroscopic and theoretical investigations were carried out, showed a strong binding of BMP-2 with NCD surfaces [25], supporting the contention that nDP could express similar properties [27]. The nDP modification of copolymer scaffolds has been shown to increase its hydrophilicity [28], facilitating stronger physisorption of rhBMP-2. An overview of different O-termination techniques facilitating surface attachment of organic groups has been reported [21]. The overall binding strength of the noncovalent interaction is governed by a multitude of individual interactions. Several forces were reported to contribute to the overall binding on NCD, such as van der Waals forces, H-bonds and electrostatic interactions. Although the release kinetics were not remarkably different between nDP-PHY and nDP-COV scaffolds, it is clear from our results that the bioactivity of rhBMP-2 was conserved on nDP-PHY scaffolds. Studies suggest that slightly acidic environments stimulate the release of proteins loaded noncovalently on nDP modified surfaces [24], a condition that was absent in our PBS buffer set-up. Body fluids aid degradation of carriers and release of BMP-2 in a variable manner, which is why comparison to the present *in vivo* results is important.

The burst release and degradation of the scaffolds might be accentuated *in vivo* [45], explaining why PHY might show higher trends of early markers such as Runx2 and COL1 *in vivo*, although the difference was not significant. Several factors play a role in bone regeneration *in vivo* [48], which could have assisted the PHY to form mineralized tissue *in vivo* but not *in vitro*. The *in vivo* experiments had different time points from the *in vitro*, bringing another variable to the effect of the release kinetics of the various scaffolds. At 2 weeks *in vivo*, the release profile showed a relatively higher release from MICS, which continued to increase, compared to PHY, and thus had a significant effect on the

Fig. 5 3D mineralization *in vitro* visualised with Alizarin red S staining. Macroscopic images (round) and increased magnifications (×4) images of (A) unseeded CL scaffold, (B) cultured hMSC for 1 week on CL scaffold (C) on PHY, (D) on nDP-PHY, (E) on nDP-COV, (F) on MICS, and (G) HOB cells on CL scaffold (positive control). Scale bar = 500 μm.3D mineralization *in vitro* visualised with Alizarin red S staining. Macroscopic images (round) and increased magnifications (×4) images of (A) unseeded CL scaffold, (B) cultured hMSC for 1 week on CL scaffold (C) on PHY, (D) on nDP-PHY, (E) on nDP-COV, (F) on MICS, and (G) HOB cells on CL scaffold (positive control). Scale bar = 500 μm.

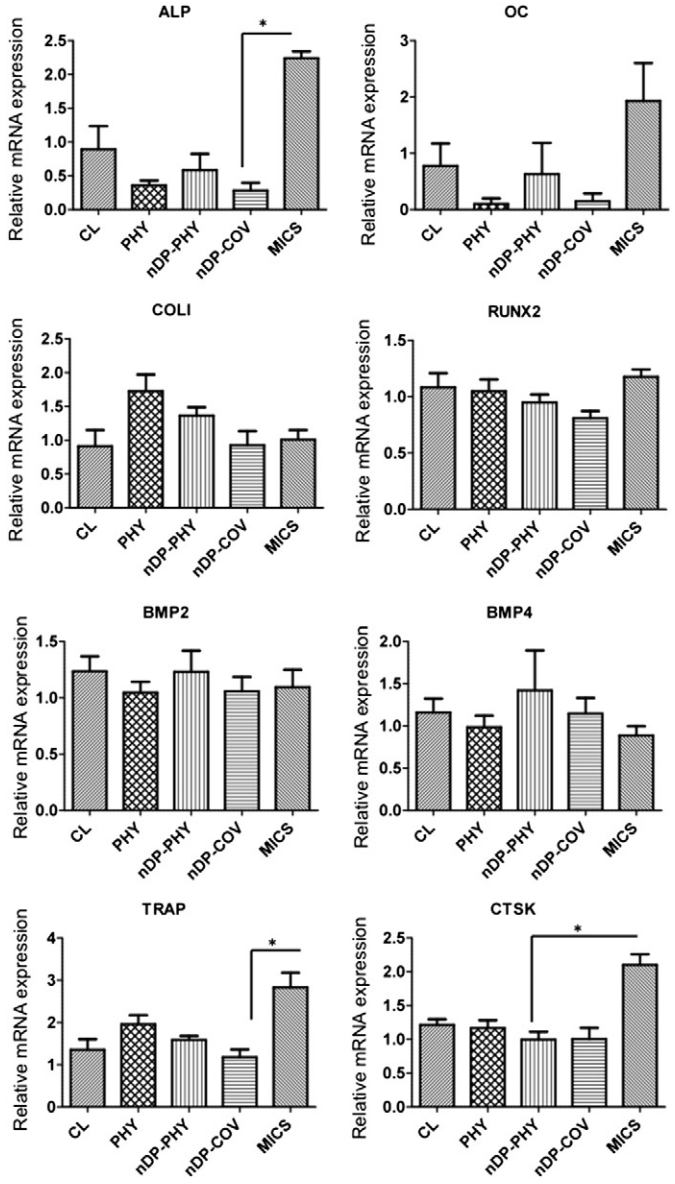

Fig. 6. Relative mRNA expression *in vivo* after week 2. Expression of BMP-2 transcription, osteogenic genes and remodelling markers by RT-PCR from animals samples after 2 weeks in place (*$p < 0.05$).

osteogenic marker, ALP. The second cross-sectional analysis *in vivo* was at four weeks which corresponds to bet'ween 21 days and 40 days of *in vitro* release kinetics. PHY and MICS showed the significantly higher bone regeneration and nDP-PHY came later, perhaps suggesting the effects of sustained release in low doses from the latter group as seen in the release curve (Fig. 1). Longer-term evaluation *in vivo* is required to fully assess the quality and architecture of new bone.

The *in vitro* results in the present study demonstrated lower ALP expression by cells grown onto MICS scaffolds than on nDP-PHY, with cells from the MICS group still significantly highly proliferative as seen by Ki67 expression at week 1, possibly related to the increased surface area from the microspheres. It has been reported that osteosarcoma cells cultured on NCD implant surfaces showed increased ALP activity in less than 2 weeks of culture [25]. *In vivo*, a significantly higher expression of mRNA ALP was demonstrated from MICS scaffolds indicating bone induction. ALP expression tended to be higher in cells on nDP-PHY scaffolds than on PHY scaffolds both *in vitro* and *in vivo*, although not significantly so, highlighting the effect of nanoparticles on enhancing the osteoinduction of copolymer scaffolds. A slight upsurge in the BMP-2 kinetic release after almost 40 days in nDP-PHY is believed to be due to the degrading polymer, but in this case the rhBMP-2 is still bound to nDP and bioactive in levels to increase osteogenic differentiation when compared with PHY scaffold. This was confirmed by Alizarin red staining in the nDP-PHY and MICS scaffold groups.

The nDP-COV group showed no release of BMP-2 during the 70 days of incubation and also showed lesser osteogenic potential both *in vitro* and *in vivo*. This demonstrates the high stability of the covalent immobilization of the protein on the diamond surface. The loss of the BMP-2 functionality indicates that the protein is most likely deformed during the binding onto the diamond surface by both the covalent linker and additional, non-covalent interactions. Similar results have been reported previously for the covalent immobilization of other proteins such as enzymes [49]. This brings to our notice the necessity of improving the method for covalently bonding the rhBMP-2 to the nDP without affecting the bioactivity of rhBMP-2. Furthermore, we take into consideration that the *in vitro* design of 3 weeks was not suitable for the nDP-COV group; additional degradation of the scaffold is required to release rhBMP-2. This was evidenced by the observation of limited osteoid tissue around the nDP areas at 4 weeks *in vivo* (Fig. 7F).

BMP-2 exerts a bipolar effect depending on its concentration: osteoprogenitor cells are recruited and differentiated at low doses, whereas osteoclasts are transiently activated at high doses [50]. This was reflected by the *in vivo* expression of TRAP and CTSK, (Fig. 6), both highly expressed by osteoclasts. They were significantly highly expressed in the MICS scaffold group after 2 weeks; *in vivo* this release could be amplified due to environments favourable to erosion of the microspheres. Recent reports [51] have underlined the importance of decreasing the dose of BMP-2 to the lowest level that is compatible with the desired effect of bone formation. BMP-2 is expressed from days 1 to 21 during bone healing [48], hence for delivering BMP-2 for bone regeneration, the ideal carrier would provide sustained release over a period of at least three weeks. Following injury, BMP-2 is released locally into the defect site from the surrounding matrix [48], consistent with the increased BMP-2 levels *in vivo* seen here in all groups, although this increase was not statistically significant. Also consistent with trends seen here, BMP-2 expression is upregulated in differentiating osteoprogenitor cells and maintained for about 21 days [52]. At week 3 *in vitro*, the highest expression was seen in the MICS ($p < 0.05$) and followed by nDP-PHY at both time points. A similar trend in the extracellular protein levels of BMP-2 was shown by ELISA. Comparing the gene and protein expressions of BMP-2 between PHY and nDP-PHY highlights the valuable effect of nDP functionalisation. BMP-2 is an extracellular signalling molecule which is washed out rapidly, thus the protein level of extra- and intra-cellular BMP-2 was reduced at week 3 in all groups [53]. Small amounts induce cellular responses *in vitro*; however exogenously delivered BMP-2 requires ultra-physiological doses for humans compared to animals to overcome the rapid wash out.

It is important to note that *in vitro* statistical relevance was seen in mRNA expressions of the potent osteogenic markers BMP-2 and OC *in vitro*, hence our discussion and subsequent conclusions are based on this finding. Significance *in vivo* was only demonstrated for ALP mRNA from MICS scaffold compared to other osteogenic markers. However, microCT and histological evaluations disclosed a confirmative dimension supporting the interpretations and conclusions related to the osteogenic potential of these scaffolds. The nDP-PHY and MICS scaffolds have strong potential for future applications due to their controlled release of growth factors. Furthermore, the data demonstrated that the protein on nDP-PHY was bioactive with comparable efficacy despite being strongly bound to the carrier (scaffolds), indicating a short distance effect on the local surrounding tissues.

In the clinical trials, high doses of not less than 1 mg BMPs per ml have been used and the complications of this dose have been discussed [54]. However, it is difficult to establish a correlation from animals to humans due to different bone healing mechanisms [55]. Interestingly,

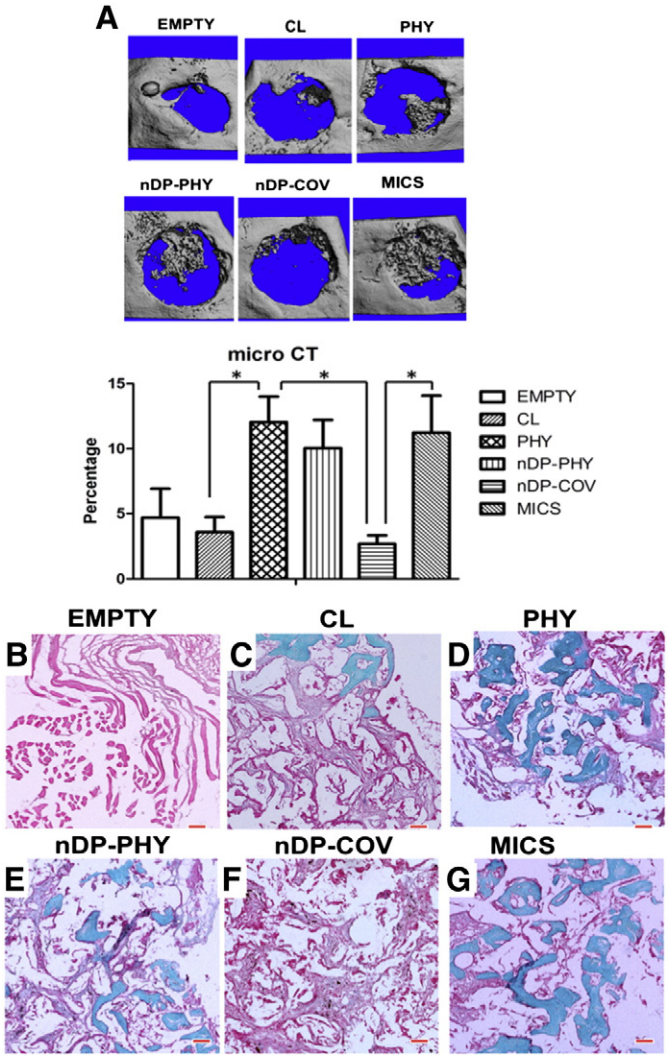

Fig. 7. *De novo* bone formation after 4 weeks post-implantation. (A) Micro-CT analysis showing different bone formation volumes inside the region of the defect at 4 weeks (*$p < 0.05$). (B–G) Masson trichrome staining of defects implanted with different scaffolds at 4 weeks post-implantation. The bluish green colour indicated osteoid-like tissue and collagen-rich areas. Scale bar = 100 μm.

in our study a low dose of only 1 μg was sufficient to induce *de novo* bone. Very few experiments using comparably low doses *in vivo* have been reported. Researchers used carrier minerals, which might have a confounding osteoinductive effect [56] or including osteoprogenitor cells in the construct [57]. A recent study using collagen sponges in critical sized defects in rat calvaria [58] concluded that rhBMP-2 accelerates local bone formation once reaching an osteoinductive dose threshold at 1.25-2.5 μg in their model, which is not load bearing. Previous reports also proved that non-glycosylated BMP-2 which is produced via bacterial expression systems is less soluble. Despite it having lower biological activity and release *in vitro* compared to glycolysated BMP-2, it significantly increased bone formation at low dosages [59].

Taken together, we conclude from our results that low doses of BMP-2 are found to be bioactive for bone regeneration. Obtaining bone after just 4 weeks *in vivo* suggests accelerated bone regeneration in the PHY, nDP-PHY and MICS groups. Physisorption onto nDP modified copolymer scaffolds is a material reported for the first time in critical sized bone defects and appears to hold great promise compared to growth factors adsorbed solely onto a polymer.

Acknowledgements

The research leading to these results has received funding by the European Union's Seventh Framework Programme under grant agreement number 242175-VascuBone. The MS work was carried out at the Proteomics Unit at UiB (PROBE) and the authors acknowledge Prof. Frode Berven, Proteomics Unit at the University of Bergen and Dr. Frank Kloss, Medical University of Innsbruck, Austria for the scientific discussions during the design of the experiments. The authors thank Dr. Michele Cottler-Fox, University of Arkansas for Medical Sciences, Little Rock, USA for English revision and constructive criticism of the manuscript.

References

[1] K. Lee, E.A. Silva, D.J. Mooney, Growth factor delivery-based tissue engineering: general approaches and a review of recent developments, J. R. Soc. Interface./R. Soc. 8 (2011) 153–170.
[2] J.E. Schroeder, R. Mosheiff, Tissue engineering approaches for bone repair: concepts and evidence, Injury 42 (2011) 609–613.
[3] Q. Zhang, Q.F. He, T.H. Zhang, X.L. Yu, Q. Liu, F.L. Deng, Improvement in the delivery system of bone morphogenetic protein-2: a new approach to promote bone formation, Biomed. Mater. 7 (2012) 045002.
[4] S. Govender, C. Csimma, H.K. Genant, A. Valentin-Opran, Y. Amit, R. Arbel, H. Aro, D. Atar, M. Bishay, M.G. Borner, P. Chiron, P. Choong, J. Cinats, B. Courtenay, R. Feibel, B. Geulette, C. Gravel, N. Haas, M. Raschke, E. Hammacher, D. van der Velde, P. Hardy, M. Holt, C. Josten, R.L. Ketterl, B. Lindeque, G. Lob, H. Mathevon, G. McCoy, D. Marsh, R. Miller, E. Munting, S. Oevre, L. Nordsletten, A. Patel, A. Pohl, W. Rennie, P. Reynders, P.M. Rommens, J. Rondia, W.C. Rossouw, P.J. Daneel, S. Ruff, A. Ruter, S. Santavirta, T.A. Schildhauer, C. Gekle, R. Schnettler, D. Segal, H. Seiler, R.B. Snowdowne, J. Stapert, G. Taglang, R. Verdonk, L. Vogels, A. Weckbach, A. Wentzensen, T. Wisniewski, B.M.P.E.i.S.f.T.T.S. Group, Recombinant human bone morphogenetic protein-2 for treatment of open tibial fractures: a prospective, controlled, randomized study of four hundred and fifty patients, J. Bone Joint Surg. 84-A (2002) 2123–2134.
[5] L.B. Shields, G.H. Raque, S.D. Glassman, M. Campbell, T. Vitaz, J. Harpring, C.B. Shields, Adverse effects associated with high-dose recombinant human bone morphogenetic protein-2 use in anterior cervical spine fusion, Spine 31 (2006) 542–547.
[6] A.C. Carreira, F.H. Lojudice, E. Halcsik, R.D. Navarro, M.C. Sogayar, J.M. Granjeiro, Bone morphogenetic proteins: facts, challenges, and future perspectives, J. Dent. Res. 93 (2014) 335–345.
[7] J.P. Issa, M.V. Bentley, M.M. Iyomasa, W. Sebald, R.F. De Albuquerque, Sustained release carriers used to delivery bone morphogenetic proteins in the bone healing process, Anat. Histol. Embryol. 37 (2008) 181–187.
[8] T.H. Kim, Y.P. Yun, Y.E. Park, S.H. Lee, W. Yong, J. Kundu, J.W. Jung, J.H. Shim, D.W. Cho, S.E. Kim, H.R. Song, *In vitro* and *in vivo* evaluation of bone formation using solid freeform fabrication-based bone morphogenic protein-2 releasing PCL/PLGA scaffolds, Biomed. Mater. 9 (2014) 025008.
[9] E.L. Hsu, J.H. Ghodasra, A. Ashtekar, M.S. Nickoli, S.S. Lee, S.I. Stupp, W.K. Hsu, A comparative evaluation of factors influencing osteoinductivity among scaffolds designed for bone regeneration, Tissue Eng. A 19 (2013) 1764–1772.
[10] G. Wu, Y. Liu, T. Iizuka, E.B. Hunziker, The effect of a slow mode of BMP-2 delivery on the inflammatory response provoked by bone-defect-filling polymeric scaffolds, Biomaterials 31 (2010) 7485–7493.
[11] D.H. Kempen, L. Lu, T.E. Hefferan, L.B. Creemers, A. Maran, K.L. Classic, W.J. Dhert, M.J. Yaszemski, Retention of *in vitro* and *in vivo* BMP-2 bioactivities in sustained delivery vehicles for bone tissue engineering, Biomaterials 29 (2008) 3245–3252.
[12] S. Asamura, Y. Mochizuki, M. Yamamoto, Y. Tabata, N. Isogai, Bone regeneration using a bone morphogenetic protein-2 saturated slow-release gelatin hydrogel sheet: evaluation in a canine orbital floor fracture model, Ann. Plast. Surg. 64 (2010) 496–502.
[13] S. Srouji, D. Ben-David, R. Lotan, E. Livne, R. Avrahami, E. Zussman, Slow-release human recombinant bone morphogenetic protein-2 embedded within electrospun scaffolds for regeneration of bone defect: *in vitro* and *in vivo* evaluation, Tissue Eng. A 17 (2011) 269–277.
[14] A. Shekaran, A.J. Garcia, Extracellular matrix-mimetic adhesive biomaterials for bone repair, J. Biomed. Mater. Res. A 96 (2011) 261–272.
[15] F. Yang, J. Wang, J. Hou, H. Guo, C. Liu, Bone regeneration using cell-mediated responsive degradable PEG-based scaffolds incorporating with rhBMP-2, Biomaterials 34 (2013) 1514–1528.
[16] H. Zhang, F. Migneco, C.Y. Lin, S.J. Hollister, Chemically-conjugated bone morphogenetic protein-2 on three-dimensional polycaprolactone scaffolds stimulates osteogenic activity in bone marrow stromal cells, Tissue Eng. A 16 (2010) 3441–3448.
[17] T.S. Tsapikouni, Y.F. Missirlis, Protein-material interactions: from micro-to-nano scale, Sci. Eng. B Adv. Funct. Solid-State Mater. 152 (2008) 2–7.
[18] S. Freiberg, X.X. Zhu, Polymer microspheres for controlled drug release, Int. J. Pharm. 282 (2004) 1–18.
[19] C. Nugraha, M. Bora, S.S. Venkatraman, Release retardation of model protein on polyelectrolyte-coated PLGA nano- and microparticles, PLoS One 9 (2014) e92393.

[20] F.R. Kloss, M. Najam-Ul-Haq, M. Rainer, R. Gassner, G. Lepperdinger, C.W. Huck, G. Bonn, F. Klauser, X. Liu, N. Memmel, E. Bertel, J.A. Garrido, D. Steinmuller-Nethl, Nanocrystalline diamond—an excellent platform for life science applications, J. Nanosci. Nanotechnol. 7 (2007) 4581–4587.
[21] A. Krueger, D. Lang, Functionality is key: recent progress in the surface modification of nanodiamond, Adv. Funct. Mater. 22 (2012) 890–906.
[22] M. Mansoorianfar, M.A. Shokrgozar, M. Mehrjoo, E. Tamjid, A. Simchi, Nanodiamonds for surface engineering of orthopedic implants: enhanced biocompatibility in human osteosarcoma cell culture, Diam. Relat. Mater. 40 (2013) 107–114.
[23] V.N. Mochalin, A. Pentecost, X.M. Li, I. Neitzel, M. Nelson, C.Y. Wei, T. He, F. Guo, Y. Gogotsi, Adsorption of drugs on nanodiamond: toward development of a drug delivery platform, Mol. Pharm. 10 (2013) 3728–3735.
[24] L. Moore, M. Gatica, H. Kim, E. Osawa, D. Ho, Multi-protein delivery by nanodiamonds promotes bone formation, J. Dent. Res. 92 (2013) 976–981.
[25] D. Steinmuller-Nethl, F.R. Kloss, M. Najam-Ul-Haq, M. Rainer, K. Larsson, C. Linsmeier, G. Kohler, C. Fehrer, G. Lepperdinger, X. Liu, N. Memmel, E. Bertel, C.W. Huck, R. Gassner, G. Bonn, Strong binding of bioactive BMP-2 to nanocrystalline diamond by physisorption, Biomaterials 27 (2006) 4547–4556.
[26] F.R. Kloss, R. Gassner, J. Preiner, A. Ebner, K. Larsson, O. Hachl, T. Tuli, M. Rasse, D. Moser, K. Laimer, E.A. Nickel, G. Laschober, R. Brunauer, G. Klima, P. Hinterdorfer, D. Steinmuller-Nethl, G. Lepperdinger, The role of oxygen termination of nanocrystalline diamond on immobilisation of BMP-2 and subsequent bone formation, Biomaterials 29 (2008) 2433–2442.
[27] A. Krueger, New carbon materials: biological applications of functionalized nanodiamond materials, Chemistry 14 (2008) 1382–1390.
[28] Z. Xing, T.O. Pedersen, X. Wu, Y. Xue, Y. Sun, A. Finne-Wistrand, F.R. Kloss, T. Waag, A. Krueger, D. Steinmuller-Nethl, K. Mustafa, Biological effects of functionalizing copolymer scaffolds with nanodiamond particles, Tissue Eng. A 19 (2013) 1783–1791.
[29] E.B. Hunziker, L. Enggist, A. Kuffer, D. Buser, Y. Liu, Osseointegration: the slow delivery of BMP-2 enhances osteoinductivity, Bone 51 (2012) 98–106.
[30] G. Bhakta, B. Rai, Z.X. Lim, J.H. Hui, G.S. Stein, A.J. van Wijnen, V. Nurcombe, G.D. Prestwich, S.M. Cool, Hyaluronic acid-based hydrogels functionalized with heparin that support controlled release of bioactive BMP-2, Biomaterials 33 (2012) 6113–6122.
[31] S. Danmark, A. Finne-Wistrand, M. Wendel, K. Arvidson, A.C. Albertsson, K. Mustafa, Osteogenic differentiation by rat bone marrow stromal cells on customized biodegradable polymer scaffolds, J. Bioact. Compat. Polym. 25 (2010) 207–223.
[32] S.B. Idris, S. Danmark, A. Finne-Wistrand, K. Arvidson, A.C. Albertsson, A.I. Bolstad, K. Mustafa, Biocompatibility of polyester scaffolds with fibroblasts and osteoblast-like cells for bone tissue engineering, J. Bioact. Compat. Polym. 25 (2010) 567–583.
[33] U. Edlund, S. Danmark, A.C. Albertsson, A strategy for the covalent functionalization of resorbable polymers with heparin and osteoinductive growth factor, Biomacromolecules 9 (2008) 901–905.
[34] T. Kirsch, J. Nickel, W. Sebald, BMP-2 antagonists emerge from alterations in the low-affinity binding epitope for receptor BMPR-II, EMBO J. 19 (2000) 3314–3324.
[35] A. Krüger, F. Kataoka, M. Ozawa, T. Fujino, Y. Suzuki, A.E. Aleksenskii, A.Y. Vul', E. Ōsawa, Unusually tight aggregation in detonation nanodiamond: identification and disintegration, Carbon 43 (2005) 1722–1730.
[36] Y. Yang, G. Tang, H. Zhang, Y. Zhao, X. Yuan, Y. Fan, M. Wang, Controlled release of BSA by microsphere-incorporated PLGA scaffolds under cyclic loading, Mater. Sci. Eng. C 31 (2011) 350–356.
[37] G. Wei, Q. Jin, W.V. Giannobile, P.X. Ma, Nano-fibrous scaffold for controlled delivery of recombinant human PDGF-BB, J. Control. Release 112 (2006) 103–110.
[38] Z.Q. Fei, Y.Y. Hu, D.C. Wu, H. Wu, R. Lu, J.P. Bai, H.X. Song, Preparation and property of a novel bone graft composite consisting of rhBMP-2 loaded PLGA microspheres and calcium phosphate cement, J. Mater. Sci. Mater. Med. 19 (2008) 1109–1116.
[39] A.C. Kroksveen, E. Aasebo, H. Vethe, V. Van Pesch, D. Franciotta, C.E. Teunissen, R.J. Ulvik, C. Vedeler, K.M. Myhr, H. Barsnes, F.S. Berven, Discovery and initial verification of differentially abundant proteins between multiple sclerosis patients and controls using iTRAQ and SID-SRM, J. Proteome 78 (2013) 312–325.
[40] Z. Xing, Y. Xue, S. Danmark, A. Finne-Wistrand, K. Arvidson, S. Hellem, Z.Q. Yang, K. Mustafa, Comparison of short-run cell seeding methods for poly(L-lactide-co-1,5-dioxepan-2-one) scaffold intended for bone tissue engineering, Int. J. Artif. Organs 34 (2011) 432–441.
[41] K. Mustafa, A. Wennerberg, J. Wroblewski, K. Hultenby, B.S. Lopez, K. Arvidson, Determining optimal surface roughness of TiO2 blasted titanium implant material for attachment, proliferation and differentiation of cells derived from human mandibular alveolar bone, Clin. Oral Implant. Res. 12 (2001) 515–525.
[42] J. Schnabl, R. Glueckert, G. Feuchtner, W. Recheis, T. Potrusil, V. Kuhn, A. Wolf-Magele, H. Riechelmann, G.M. Sprinzl, Sheep as a large animal model for middle and inner ear implantable hearing devices: a feasibility study in cadavers, Otol. Neurotol. 33 (2012) 481–489.
[43] Z. Xing, Y. Xue, S. Danmark, K. Schander, S. Ostvold, K. Arvidson, S. Hellem, A. Finne-Wistrand, A.C. Albertsson, K. Mustafa, Effect of endothelial cells on bone regeneration using poly(L-lactide-co-1,5-dioxepan-2-one) scaffolds, J. Biomed. Mater. Res. A 96 (2011) 349–357.
[44] S.A. Gerber, J. Rush, O. Stemman, M.W. Kirschner, S.P. Gygi, Absolute quantification of proteins and phosphoproteins from cell lysates by tandem MS, Proc. Natl. Acad. Sci. U. S. A. 100 (2003) 6940–6945.
[45] S. Danmark, A. Finne-Wistrand, K. Schander, M. Hakkarainen, K. Arvidson, K. Mustafa, A.C. Albertsson, *In vitro* and *in vivo* degradation profile of aliphatic polyesters subjected to electron beam sterilization, Acta Biomater. 7 (2011) 2035–2046.
[46] O. Jeon, S.J. Song, H.S. Yang, S.H. Bhang, S.W. Kang, M.A. Sung, J.H. Lee, B.S. Kim, Long-term delivery enhances *in vivo* osteogenic efficacy of bone morphogenetic protein-2 compared to short-term delivery, Biochem. Biophys. Res. Commun. 369 (2008) 774–780.
[47] J. Mona, C.J. Kuo, E. Perevedentseva, A.V. Priezzhev, C.L. Cheng, Adsorption of human blood plasma on nanodiamond and its influence on activated partial thromboplastin time, Diam. Relat. Mater. 39 (2013) 73–77.
[48] M. Mehta, K. Schmidt-Bleek, G.N. Duda, D.J. Mooney, Biomaterial delivery of morphogens to mimic the natural healing cascade in bone, Adv. Drug Deliv. Rev. 64 (2012) 1257–1276.
[49] K. Goldberg, A. Krueger, T. Meinhardt, W. Kroutil, B. Mautner, A. Liese, Novel immobilization routes for the covalent binding of an alcohol dehydrogenase from *Rhodococcus ruber* DSM 44541, Tetrahedron Asymmetry 19 (2008) 1171–1173.
[50] M. Okamoto, J. Murai, H. Yoshikawa, N. Tsumaki, Bone morphogenetic proteins in bone stimulate osteoclasts and osteoblasts during bone development, J. Bone Miner. Res. Off. J. Am. Soc. Bone Miner. Res. 21 (2006) 1022–1033.
[51] S. Granholm, P. Henning, C. Lindholm, U.H. Lerner, Osteoclast progenitor cells present in significant amounts in mouse calvarial osteoblast isolations and osteoclastogenesis increased by BMP-2, Bone 52 (2013) 83–92.
[52] Z. Huang, E.R. Nelson, R.L. Smith, S.B. Goodman, The sequential expression profiles of growth factors from osteoprogenitors [correction of osteroprogenitors] to osteoblasts in vitro, Tissue Eng. 13 (2007) 2311–2320.
[53] E. Birmingham, G.L. Niebur, P.E. McHugh, G. Shaw, F.P. Barry, L.M. McNamara, Osteogenic differentiation of mesenchymal stem cells is regulated by osteocyte and osteoblast cells in a simplified bone niche, Eur. Cells Mater. 23 (2012) 13–27.
[54] M.C. Simmonds, J.V.E. Brown, M.K. Heirs, J.P.T. Higgins, R.J. Mannion, M.A. Rodgers, L.A. Stewart, Safety and effectiveness of recombinant human bone morphogenetic protein-2 for spinal fusion: a meta-analysis of individual-participant data, Ann. Intern. Med. 158 (2013) 877- +.
[55] V.E. Santo, M.E. Gomes, J.F. Mano, R.L. Reis, Controlled release strategies for bone, cartilage, and osteochondral engineering–Part II: challenges on the evolution from single to multiple bioactive factor delivery, Tissue Eng. B Rev. 19 (2013) 327–352.
[56] Y. Liu, K. de Groot, E.B. Hunziker, BMP-2 liberated from biomimetic implant coatings induces and sustains direct ossification in an ectopic rat model, Bone 36 (2005) 745–757.
[57] S. Jo, S. Kim, T.H. Cho, E. Shin, S.J. Hwang, I. Noh, Effects of recombinant human bone morphogenic protein-2 and human bone marrow-derived stromal cells on *in vivo* bone regeneration of chitosan-poly(ethylene oxide) hydrogel, J. Biomed. Mater. Res. A 101 (2013) 892–901.
[58] M. Pelaez, C. Susin, J. Lee, T. Fiorini, F.C. Bisch, D.R. Dixon, J.C. McPherson, A.N. Buxton III, U.M. Wikesjo, Effect of rhBMP-2 dose on bone formation/maturation in a rat critical-size calvarial defect model, J. Clin. Periodontol. 41 (2014) 827–836.
[59] F.C.J. van de Watering, J. van den Beucken, S.P. van der Woning, A. Briest, A. Eek, H. Qureshi, L. Winnubst, O.C. Boerman, J.A. Jansen, Non-glycosylated BMP-2 can induce ectopic bone formation at lower concentrations compared to glycosylated BMP-2, J. Control. Release 159 (2012) 69–77.